CSnrc: Correlated sampling Monte Carlo calculations using EGSnrc

Lesley A. Buckley[a)]
Ionizing Radiation Standards, National Research Council of Canada, 1200 Montreal Road, Building M-35, Ottawa K1A OR6, Canada and Ottawa-Carleton Institute of Physics, Carleton University, Ottawa K1S 5B6, Canada

I. Kawrakow
Ionizing Radiation Standards, National Research Council of Canada, 1200 Montreal Road, Building M-35, Ottawa K1A OR6, Canada

D. W. O. Rogers
Ottawa-Carleton Institute of Physics, Carleton University, Ottawa K1S 5B6, Canada

(Received 9 July 2004; revised 25 August 2004; accepted for publication 20 September 2004; published 23 November 2004)

CSnrc, a new user-code for the EGSnrc Monte Carlo system is described. This user-code improves the efficiency when calculating ratios of doses from similar geometries. It uses a correlated sampling variance reduction technique. CSnrc is developed from an existing EGSnrc user-code CAVRZnrc and improves upon the correlated sampling algorithm used in an earlier version of the code written for the EGS4 Monte Carlo system. Improvements over the EGS4 version of the algorithm avoid repetition of sections of particle tracks. The new code includes a rectangular phantom geometry not available in other EGSnrc cylindrical codes. Comparison to CAVRZnrc shows gains in efficiency of up to a factor of 64 for a variety of test geometries when computing the ratio of doses to the cavity for two geometries. CSnrc is well suited to in-phantom calculations and is used to calculate the central electrode correction factor P_{cel} in high-energy photon and electron beams. Current dosimetry protocols base the value of P_{cel} on earlier Monte Carlo calculations. The current CSnrc calculations achieve 0.02% statistical uncertainties on P_{cel}, much lower than those previously published. The current values of P_{cel} compare well with the values used in dosimetry protocols for photon beams. For electrons beams, CSnrc calculations are reported at the reference depth used in recent protocols and show up to a 0.2% correction for a graphite electrode, a correction currently ignored by dosimetry protocols. The calculations show that for a 1 mm diameter aluminum central electrode, the correction factor differs somewhat from the values used in both the IAEA TRS-398 code of practice and the AAPM's TG-51 protocol. © *2004 American Association of Physicists in Medicine.* [DOI: 10.1118/1.1813891]

Key words: correlated sampling, Monte Carlo, dosimetry

I. INTRODUCTION

Monte Carlo calculations are widely used in radiation dosimetry for the determination of a wide variety of correction factors. Such calculations can be used to simulate in-phantom dosimeter response. These types of calculations are difficult, since they require hundreds of millions of particle histories in order to achieve reasonable statistical uncertainties in the results. The difficulties in simulating ion chamber response in large phantoms are illustrated by the calculations performed by Nilsson *et al.*[1] and Andreo *et al.*[2] which demonstrate the need for variance reduction techniques beyond those normally used.[3,4]

In the early 1990s, Ma and Nahum[5,6] described a correlated sampling variance reduction technique that could be used to address such problems. In subsequent papers, this technique was used for calculation of correction factors in ion chamber calculations and in Fricke dosimetry.[7–9] In general, correlated sampling is useful in situations where the ratio of, or difference between, certain quantities, due to differences in the simulation geometries, is of interest. It is of particular interest in cases where the difference between the geometries is small. For example, in the case of an in-phantom, ion chamber calculation, the majority of the geometry may stay the same and two geometries may differ only in the material or thickness of the chamber wall.

Correlated sampling exploits correlations between similar geometries to reduce the uncertainty on the ratio or difference of calculated quantities and reduces the total time required for the simulations. Correlated sampling may therefore be used to improve the efficiency of calculations involving correlated quantities.[5,10] Consider, for example, a quantity that is to be calculated for two different geometries. It is straightforward to simply execute the Monte Carlo calculation twice and compare the results. If, however, the difference between the two sets of results is small, the calculations must achieve very small statistical uncertainties in order to perform a meaningful comparison. The computation time therefore becomes very large since the problem requires two separate calculations with very low statistical uncertainties. To improve upon the efficiency of this type of problem, correlated sampling uses a single execution of the Monte Carlo calculations and uses similar particle trajectories for

the two geometries. This reduces the total computation time since the entire simulation does not have to be performed twice. Furthermore, if the two geometries are similar, the two results are correlated, and they will deviate from their respective expectation values in the same direction, thereby reducing the uncertainty on the resulting difference or ratio of the two values.

A variety of correlated sampling methods have been employed for radiation dosimetry applications. Bielajew[11] employed a method whereby the initial random number seeds were stored for any history in which the primary particle, or any secondary particles, deposited dose in the cavity. This history was then repeated with the same initial seeds for each of the additional geometries. This method has the disadvantage of repeating entire histories, even when only a small fraction of the transport occurs in a region that has changed from the previous geometry. Furthermore, histories that do not result in dose deposition in the initial geometry are not repeated,[11] but some of these histories may have deposited energy in subsequent geometries. In most cases, this has been shown to have no significant effect on the results.[5]

Hedtjärn *et al.*[12] applied a fixed-collision correlated sampling technique[13] to photon transport for brachytherapy applications. In this method, the correlated sampling region is treated as a perturbation to a homogeneous geometry. A set of histories is generated for the homogeneous case, and then the histories are rescored for the perturbed case, using weighting factors for the photon collisions. For realistic photon collision physics in this method, some complicated problems must be solved in order to compute the weighting factors for the heterogeneous cases, however a high degree of correlation is maintained, as the entire history is correlated between geometries.

The correlated sampling method described here is based upon the method developed by Ma and Nahum[5] for ion chamber calculations, and by Holmes *et al.*[10] for electron beam dose calculations. In this method, histories are followed until they encounter the boundary of the region which varies between geometries, they are then split, and the simulation continues independently for each geometry. Unlike the method described by Bielajew,[11] entire histories are not repeated in this approach. This correlated sampling algorithm also has the advantage of being very straightforward to implement and does not require complicated calculations of weighting factors as described above. Changes from this earlier version of the code to the present EGSnrc version overcome some of the disadvantages of the method used by Ma and Nahum. These changes will be described in a subsequent section.

This paper describes the implementation of the correlated sampling method within the EGSnrc Monte Carlo code system.[14,15] EGSnrc is the first Monte Carlo code able to simulate ion chamber response to an accuracy of 0.1%, at least with respect to its own cross-sections and geometry descriptions.[16] The correlated sampling user-code in the EGSnrc system CSnrc is developed from an existing user-code CAVRZnrc,[17] and, although changed substantially, is based upon the earlier correlated sampling code,[5] which was similarly based on the earlier CAVRZ user-code, written for the EGS4 Monte Carlo code system.[18]

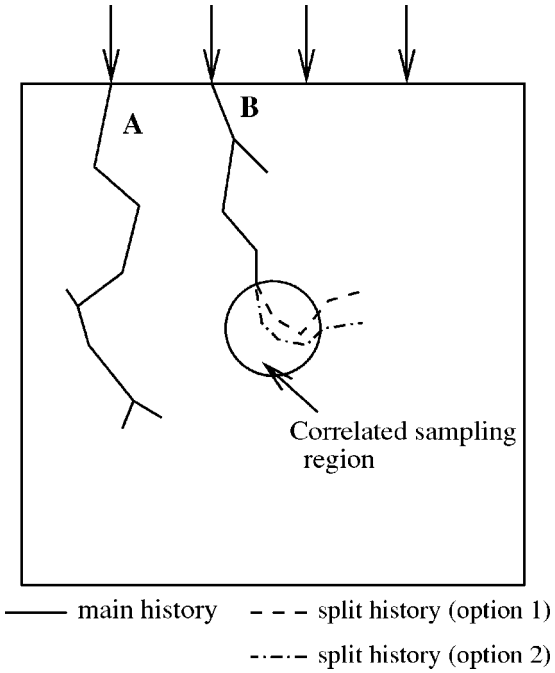

FIG. 1. Schematic demonstrating the correlated sampling method. The small region within the larger phantom is the correlated sampling region and changes material with each new geometry option. Particle A shows a main history that never enters the correlated sampling region and is transported only once during the entire simulation. Particle B shows a particle for which the main history (solid line) is transported only once, and the split history (dashed lines) transport is repeated for each geometry option. For positive correlations, the trajectories will be similar for each of the geometry options.

Using CSnrc, it is possible to improve upon calculations performed using earlier versions of the code. This paper describes calculations of the central electrode correction factor for thimble ionization chambers using CSnrc. These calculations achieve much lower statistical uncertainties than previous calculations and present a complete set of values, calculated at the currently used reference depths so they can be compared with the values currently used in dosimetry protocols.[19,20]

II. METHODS

A. Correlated sampling method

The correlated sampling method used in EGSnrc is best illustrated by considering an example. Figure 1 shows a small region at some depth within a rectangular phantom. In a given simulation, the correlated sampling regions are defined as those regions that differ between geometries. In Fig. 1, if the problem of interest is to compare the dose to the small region for different materials in the region, the small region is defined as the correlated sampling (CS) region. Instead of performing the entire calculation multiple times, each time changing the material within the small region, CSnrc calculates the dose to the CS region for all of the different cases with a single execution of the code.

For each history, the particle is followed as a main history until it enters the correlated sampling region, at which point it is separated into the distinct geometry options. Track A shows a particle that travels through the phantom without ever entering the CS region. For these particles, the simulation is only performed once, potentially resulting in significant time savings. Track B is transported as a main history only until it reaches the boundary of the CS region. Following the step to the boundary, once the particle has entered the correlated sampling region, the particle data and the state of the random number generator are stored. The rest of the particle trajectory continues as before, with all dose being scored to the first geometry option. The particle and any secondary particles produced are scored to the first geometry option until the completion of their transport, regardless of whether or not they leave the CS region. When the particle and its descendants have been transported for the first geometry, the particle data are restored to the point in the main history where the split began. The particle is once again transported, this time with the material in the CS region being that of the second geometry option, and the dose is scored for the second option. This continues for all of the geometry options, and when all transport has been completed for that history, the next history begins as a main history.

Clearly, there will be some savings in execution time since particles that never enter the correlated sampling region are only transported once, regardless of the number of geometries. Similarly, for a large phantom, the transport that takes place in the phantom, before the particle enters the correlated sampling region, is not repeated for each option. The greatest gain in computing efficiency however, comes from the reduction in the uncertainty on the ratio of scored quantities in the multiple geometries. Consider track B in Fig. 1. At the point where the particle enters the correlated sampling region, it has certain position and direction coordinates and a given energy. Based on these characteristics, the particle may result in energy deposition in the CS region. If the region's material is then changed, the particle is still entering the correlated sampling region with the same parameters and will follow a similar trajectory. It is therefore very likely that it will also deposit energy in the region for the second geometry, particularly if the cavity materials in the two geometries have similar physical properties. The energy deposition in the CS region for the two cases is said to be positively correlated.

B. Considerations in the user-code

Within the CAVRZnrc user-code itself, the implementation of the correlated sampling algorithm with the EGSnrc code requires an additional dimension for many scoring arrays in order to differentiate between geometry options when scoring. Several flags are also introduced to distinguish between geometry options. Before the call to SHOWER, a macro, $CS-FIRST-PARTICLE, checks if the particle is starting in a correlated sampling region. In that case, all of the particle data and the state of the random number generator are saved, before beginning transport. In such cases, since the entire particle trajectory must be repeated for each geometry, the only gain in computing efficiency comes about from positive correlation in the geometries.

The implementation of correlated sampling also requires two additional macros: $CS-TAKE-DOWN-DATA and $CS-END-OF-OPTION. In the EGS4 version, these macros were inserted into the EGS4 subroutines ELECTR, PHOTON, and SHOWER. In addition to requiring changes to the EGS4 system itself, this method of implementation also resulted in some unnecessary repetition of segments of particle trajectories. For a particle that did not begin in a correlated sampling region, $CS-TAKE-DOWN-DATA stored the particle data and the state of the random number generator at the beginning of each new particle loop in ELECTR and PHOTON. For electrons, this meant that several steps often took place before the electron reached the boundary of the correlated sampling region. When the particle was restored for the next geometry option, this led to part of the trajectory being repeated within the main history. Although no duplicate scoring occurred, this was not the most efficient algorithm with respect to computation time. The EGS4 implementation of the code also resulted in numerous occurrences of the $CS-TAKE-DOWN-DATA macro, so that the particle data and random number generator information were being stored each time the new particle loop was started, and not only in the cases where the particle was entering a correlated sampling region.

In the present code the particle is forced to be treated as a "new" particle each time it crosses the boundary into a correlated sampling region. This method allows the particle data to be taken down only at the end of a step in which the particle has entered a correlated sampling region. In this way, no part of the particle trajectory is repeated outside of the correlated sampling region, and the particle data is only stored once. Furthermore, the correlated sampling macros are located in the AUSGAB subroutine in the user-code, therefore no changes to the EGSnrc system code are necessary. This implementation is possible with the new EGSnrcMP version of the Monte Carlo code,[21] since local variables are not allocated statically as they were in EGS4 and in previous versions of the EGSnrc code. This permits recursive invocation of the transport routines, ELECTR and PHOTON. Table I summarizes the three macros used in the correlated sampling algorithm and their functions.

Further changes to the CAVRZnrc user-code include the addition of a rectangular phantom geometry to the current cylindrically symmetric geometries. Since one of the problems for which correlated sampling is of greatest value is an in-phantom ion chamber calculation, the geometry must accommodate a cylindrical ion chamber within a rectangular phantom. As in other EGSnrc cylindrical geometry user-codes, the ion chamber is positioned along the z axis. Three geometrical inputs are read by the INPUTS subroutine: The thickness of the phantom (along the y axis), the width of the phantom (along the x axis), and the depth of the ion chamber within the phantom (along the y axis). An additional material input is also required to specify the phantom material.

TABLE I. Summary of the three principle macros inserted in the user-code for the implementation of the correlated sampling algorithm with EGSnrc.

Macro	Description
$CS-FIRST-PARTICLE	Inserted in main routine before call to SHOWER. Takes down particle information if particle starts in correlated sampling region.
$CS-TAKE-DOWN-DATA	Located in AUSGAB in a block that is only reached by particles that have completed a step into a correlated sampling region. Takes down all particle information and the state of the random number generator.
$CS-END-OF-OPTION	Inserted in AUSGAB following calls to PHOTON and ELECTR. Checks to see if one option has finished and increments flag to signal the next geometry. Exits the loop when transport for all geometry options is complete.

Changes in the subroutine HOWNEAR are used to calculate the distance to the rectangular boundary when a particle is in the phantom.

Minor changes are also made in a number of other auxiliary EGSnrc subroutines. Since the state of the random number generator must be recorded for each particle in the simulation, new random number storage macros are added in order to write the state of the random number generator to internal variables. New source macros are also required to accommodate a source incident on a rectangular geometry.

The CSnrc code also includes an option to vary the photon cross-sections by a user-specified amount. Two optional inputs specify whether or not the cross-sections are to be changed and by what percentage they should be changed. This feature is used for uncertainty analysis in determining the effect of uncertainties in the photon cross-sections on the calculated values.[22]

CSnrc includes the photon splitting variance reduction technique used in CAVRZnrc and described elsewhere.[4,17] The efficiency gain achieved by photon splitting is dependent upon the geometry and on the calculation parameters. For the in-phantom calculations considered here, the efficiency gain due to splitting alone was between a factor of 2 and 3 for a splitting number of 130. For these geometries, the efficiency gain was seen to show little dependence on the splitting number for values of the splitting number between 100 and 130.

C. Statistics of correlated quantities

1. Ratios of correlated quantities

Within each geometry, statistical uncertainties are computed as they are in other EGSnrc user-codes, using the history-by-history method described elsewhere.[23] The correlated sampling method is often used to compute a ratio of results from different geometries. Each geometry option has its own result and uncertainty, and since the results between options are correlated, the uncertainty estimate on the ratio of these results is computed using

$$\frac{s_{\bar{R}}}{\bar{R}} = \sqrt{\left(\frac{s_{\bar{x}}}{\bar{x}}\right)^2 + \left(\frac{s_{\bar{y}}}{\bar{y}}\right)^2 - \frac{2\,\mathrm{cov}(x,y)}{(N-1)(\bar{x}\bar{y})}}, \tag{1}$$

where $s_{\bar{x}}$ and $s_{\bar{y}}$ are the estimates of the uncertainties on $\bar{x}$ and $\bar{y}$, $\bar{R}=\bar{x}/\bar{y}$ and $\mathrm{cov}(x,y)$ is the covariance of x and y. In the context of correlated sampling, x and y refer to the same quantity, scored for two different geometries. The covariance is given by

$$\mathrm{cov}(x,y) = \frac{\sum_{i=1}^{N} x_i y_i}{N} - \frac{\sum_{i=1}^{N} x_i \sum_{i=1}^{N} y_i}{N^2}, \tag{2}$$

where N is the number of histories. Clearly, a positive covariance results in an uncertainty on the dose ratio that is lower than it would be for an uncorrelated situation, for which the covariance is 0.

2. Correlation coefficient

The degree of correlation between x and y can be evaluated using the correlation coefficient, ρ_{xy}. The correlation coefficient lies in the range $-1 \leqslant \rho \leqslant 1$ and is related to the covariance of x and y by

$$\rho_{xy} = \frac{\mathrm{cov}(x,y)}{s_{\bar{x}} s_{\bar{y}}}. \tag{3}$$

It can be seen from Eq. (1), that for a greater correlation between x and y, the uncertainty on R will be lower. Two quantities are said to be positively correlated if finding x above the mean increases the likelihood of finding y above the mean value. Conversely, a negative correlation implies that if x is found above the mean, the likelihood of finding y below the mean is increased. For correlated sampling as it is applied in CSnrc, the correlation is positive, so values of $0 \leqslant \rho \leqslant 1$ are expected.

TABLE II. Description of the seven test cases used to benchmark the CSnrc code. The region that changes materials is the correlated sampling region. For all test cases using an ionization chamber, the central electrode is 19 mm long and has a diameter of 1 mm and the air cavity is 20 mm long and 6.3 mm in diameter. The fractional increase in time for the additional geometry α and the correlation coefficient ρ are also shown.

Label	Description	α	ρ
A	Alanine pellets, 5 cm deep in a cylindrical water phantom, in a ^{60}Co beam. Alanine is replaced by water for the 2nd geometry. The pellets are 1.8 cm long and 0.25 cm in radius.	0.018	0.97
B	Thimble chamber, free in air, with an aluminum central electrode and either aluminum or graphite walls, 0.5 g/cm^2 thick. A ^{60}Co beam is incident from the side and the dose is scored to the air cavity.	0.98	0.19
C	Same as in B, but chamber walls are graphite and the electrode is either graphite or aluminum.	0.099	0.91
D	Same as in C, but the incident beam is a 10 MeV electron beam.	0.079	0.92
E	Thimble chamber with ^{60}Co beam incident from side. A 0.05 g/cm^2 wall is either graphite or aluminum and there is a graphite build-up cap to achieve full build-up.	0.69	0.26
F	Same chamber as in B, but the chamber (with no build-up cap) is placed 10 cm deep in a 30 cm cubic water phantom and the incident beam is a 10 MV photon beam. The wall material changes from graphite to water.	0.070	0.36
G	Cylindrical Al_2O_3 pellet, 2 mm in length and having a radius of 0.564 mm. The pellet is 10 cm deep in a 30 $\times 30 \times 30$ cm^3 water phantom and the incident beam is ^{60}Co.	0.0035	0.75

3. χ^2 test

In order to verify that the statistics on the ratios of correlated quantities are being estimated accurately, the χ^2 per degree of freedom is computed for a number of separate simulations using:

$$\frac{\chi^2}{df} = \frac{1}{n-1}\sum_{i=1}^{n}\frac{(R_i - \overline{R})^2}{s_{R_i}^2}, \tag{4}$$

where n is the number of simulations, $R_i = \overline{x_i}/\overline{y_i}$ is the ratio computed in simulation i, s_{R_i} is the estimated uncertainty on R_i, and $\overline{R}$ is the ratio, averaged over all n simulations, as follows:[13]

$$\overline{R} = \frac{\sum_{i=1}^{n}\overline{x_i}}{\sum_{i=1}^{n}\overline{y_i}}. \tag{5}$$

If the uncertainty is estimated accurately, χ^2/df should be ≈ 1. If the uncertainty has been underestimated, we will find $\chi^2/df \gg 1$, whereas a $\chi^2/df \ll 1$ indicates that the uncertainty has been overestimated.

4. Efficiency of Monte Carlo calculations

The efficiency, ϵ of a Monte Carlo calculation is inversely proportional to the total CPU time T and the estimated variance s^2 of the quantity being calculated

$$\epsilon = \frac{1}{s^2 T}. \tag{6}$$

The gain in efficiency provided by a variance reduction technique, compared to a conventional calculation is defined as the ratio of the efficiencies of the two methods.

III. RESULTS

A. Benchmarking tests

1. Comparison to CAVRZnrc

The first step in benchmarking the code is to ensure that the cavity dose for a given geometry option, the ratio of cavity doses for different geometries, and the statistics on the dose ratios are being computed properly. To this end, seven test input files were developed, ranging in complexity from simple in-air thimble chamber calculations, to alanine pellets in a cylindrical water phantom, to an in-phantom ion chamber calculation. The test cases differed in the type of incident beam and in which region was designated as the correlated sampling region. Table II provides a brief summary of the seven test cases.

The correlated sampling code was developed from the CAVRZnrc user-code and therefore, within their uncertainties, the two codes should give the same cavity doses for a given geometry. In order to compare the CSnrc results to those from CAVRZnrc, CSnrc was executed for each of the seven test examples and the ratio of dose to the cavity for the

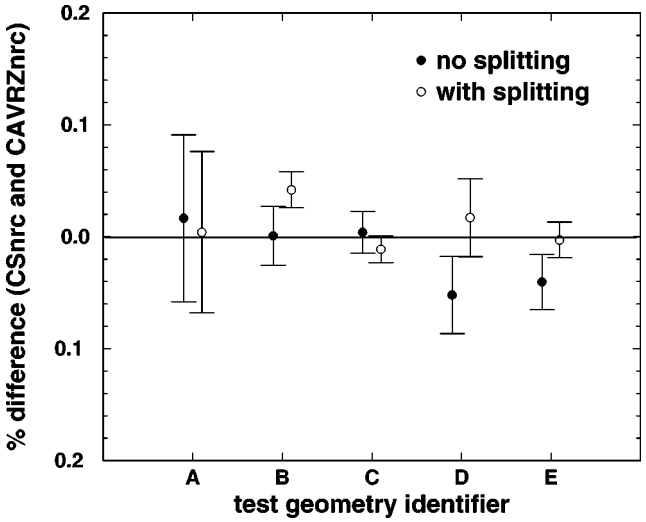

FIG. 2. The percent difference between the dose ratios computed using CSnrc and those from CAVRZnrc. The uncertainty on the percent difference is computed using standard error propagation techniques. The results are shown for five test geometries discussed in the text and are shown with and without photon splitting as an additional variance reduction technique. The two test geometries that use a rectangular phantom are not included here as this geometry is not supported by CAVRZnrc. All calculations used $AE = 521$ keV.

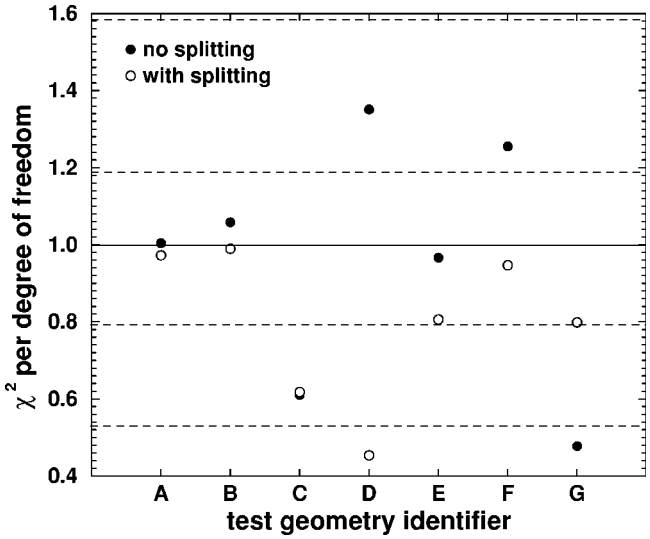

FIG. 3. Plot showing the χ^2 per degree of freedom computed for 20 independent runs used to compute the ratio of doses for two correlated geometries in the seven test cases. The dashed lines show the 68% and 95% confidence limits for the χ^2 distribution. A $\chi^2/df \approx 1$ indicates accurate estimates of the statistics on the dose ratios. The calculations were performed with (open circles) and without (solid circles) photon splitting as an added variance reduction technique.

two geometries was computed. For each of the test cases, CAVRZnrc was then executed twice, once for each geometry option, and the ratio of cavity doses was computed manually, with the uncertainty being computed as the sum of the squares of the individual dose uncertainties. The percent difference between the dose ratios from the two user-codes are shown in Fig. 2, with and without photon splitting. CSnrc gives the same results as CAVRZnrc, well within the uncertainties of 0.01% to 0.1%, the average difference having a magnitude of 0.03%. The individual cavity doses computed using the two codes also agree in all cases to within 0.1% with an average difference of 0.03%. The comparison cannot be made for the last two test cases, F and G, since CAVRZnrc does not support the use of a rectangular phantom geometry.

In addition to verifying agreement between CSnrc and CAVRZnrc, the statistics on the calculated dose ratios must be verified. For each test case, the ratio of doses to the cavity for two correlated geometries was computed in each of 20 independent runs. Using the uncertainty on the dose ratio, the χ^2 per degree of freedom was computed and is plotted in Fig. 3 along with the 68% and 95% confidence limits. As expected, for all tests, $\chi^2/df \approx 1$, and the scatter of points about $\chi^2/df = 1$ shows that there is no systematic error in the calculation of the statistics on the dose ratios, and therefore they are being calculated correctly. The calculations were performed with a low electron energy cutoff AE of 521 keV, and both with and without photon splitting as an added variance reduction technique. Where splitting was used, the splitting factor was 130. For all subsequent calculations, photon splitting is used in addition to correlated sampling in order to improve the calculation efficiency.

2. Efficiency gain

It is possible to determine the gain in efficiency achieved by using CSnrc to compute the ratio of doses for two distinct geometries instead of executing CAVRZnrc for each geometry of interest and then computing the dose ratio. Using the formalism of Ma and Nahum[5] (with an obvious correction), the efficiency gain, G, is given by

$$G = \frac{k}{1 + \alpha(k-1)} \frac{s^2_{\text{uncorr}}}{s^2_{\text{corr}}}, \tag{7}$$

where k is the number of geometry options being considered in a single execution of CSnrc, α is the fractional increase in time for each geometry option beyond the first one, and s^2_{uncorr} and s^2_{corr} are the uncertainty estimates on the dose ratios for the uncorrelated (CAVRZnrc) and correlated (CSnrc) cases, respectively. This assumes that for the same number of histories, the computation time required for an independent run of a single geometry option is the same, regardless of which geometry is being considered. For the cases considered here, values of α vary from 0.004 to 0.98 and are shown in Table II. As expected, for geometries in which the source is incident upon the correlated sampling region, α is large since the entire history is repeated and there is no savings in time. Conversely, for in-phantom calculations, where large parts of the particle trajectories are outside of the correlated sampling region, α is very small. In order to include the rectangular phantom geometries, which cannot currently be computed using CAVRZnrc, α is computed by comparing the CPU times for a CSnrc calculation using two geometries with a CSnrc calculation with correlated sampling turned off. Compared to CAVRZnrc, CSnrc used with no correlated sampling takes slightly longer due to several conditions in

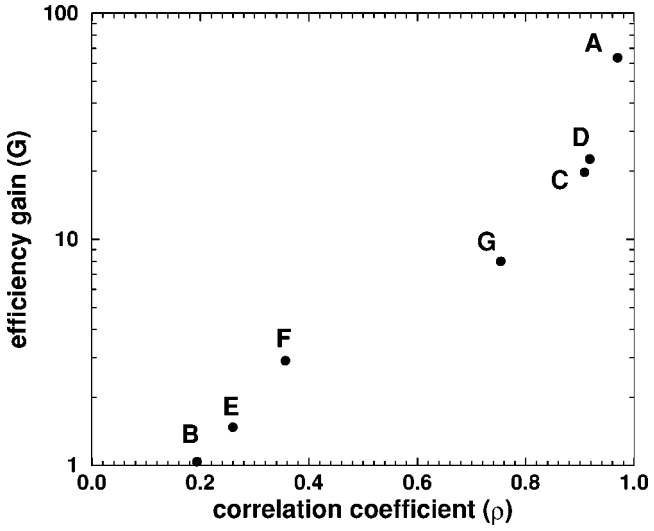

FIG. 4. Gain in efficiency achieved by CSnrc compared to CAVRZnrc, as a function of the degree of correlation between geometry options. The efficiency is computed for the calculation of the ratio of doses to the cavity for two geometry options. The calculations are performed using photon splitting with a splitting number of 130. The labels refer to the test geometries in Table II.

the code that are used to verify whether or not correlated sampling is being used. For the geometries considered here that could be used with both user-codes, CSnrc took between 3% and 10% longer than CAVRZnrc for a dose calculation for a single geometry.

The efficiency gain is expected to increase as the degree of correlation increases. For the seven test cases discussed previously, Fig. 4 shows the gain in efficiency of CSnrc over CAVRZnrc as a function of the correlation coefficient, ρ. As expected, the gain increases with increasing ρ. Each of the calculations was performed using only two geometry options. A further gain, up to a factor of 3 above the gains shown in Fig. 4, can be achieved when executing CSnrc with as many as ten geometry options, since, as k increases in Eq. (7), there is a greater savings in CPU time as more geometries are considered.

Figure 4 shows that for cases that show a reasonable degree of correlation, the efficiency gains vary between 8 and 64. Ma and Nahum[5] report typical efficiency gains of 10 to 100 for a single additional geometry using a thimble chamber geometry. Similarly, Holmes *et al.*[10] report mean efficiency gains of 2 to 200 for electron-beam calculations. More recent calculations by Hedtjärn *et al.*[12] also show efficiency gains between 10 and 100 for most cases. For some very simple slab geometries that show a high degree of correlation ($\rho=0.996$), the gain is as high as 400 using CSnrc.

The efficiency gain achieved by correlated sampling leads to much lower statistical uncertainties on calculated ratios. For a ^{60}Co beam, incident from the side on a graphite-walled thimble chamber in air, it is possible to compute the effect of using an aluminum central electrode rather than a graphite electrode. A calculation using CSnrc results in a value of $D_{gr}/D_{Al}=0.9927\pm0.0001$. This compares with, but shows much lower uncertainty than, a previous CAVRZnrc calculation[24] and with an EGS4/PRESTA correlated sampling calculation[7] that gave values of 0.9937 ± 0.0010 and 0.9942 ± 0.0013, respectively. It also agrees with the measured result of 0.992 ± 0.002 from Palm and Mattsson.[25] The CSnrc calculations use an electron cutoff energy $AE=512$ keV and a photon splitting factor of 130. The ^{60}Co spectrum used is described elsewhere.[26]

Using the same geometry, a current calculation using CAVRZnrc gives a value of $D_{gr}/D_{Al}=0.9927\pm0.0004$. Table III compares the results from CSnrc to those from the current CAVRZnrc calculation. The fractional increase in CPU time required for the additional geometry in CSnrc, α, is 0.098. Using Eq. (6), the efficiency gain in using CSnrc rather than CAVRZnrc, for this example, is $G=21$.

3. Comparison to EGS4

A previous investigation using the EGS4 correlated sampling code, studied the electrode effect in an NE2561 chamber as a function of incident electron energy.[7] Using the current CSnrc code, this study is repeated. In accordance with the study by Ma and Nahum,[7] a modified NE2561 geometry is used, and the chamber is modeled to have a wall thickness of 0.090 g/cm^2, with a sensitive air cavity 9.0 mm in length and having a diameter of 7.4 mm. The central electrode is hollow and has an outer diameter of 1.76 mm and an inner diameter of 1.4 mm, with a length of 6.4 mm. The chamber was placed in air, with a broad, parallel beam of monoenergetic electrons incident from the side. All calculations use

TABLE III. Comparison of the dose ratio D_{gr}/D_{Al} for a graphite-walled thimble chamber, computed using CAVRZnrc and CSnrc. The dose ratio compares the dose to the cavity for a chamber having a graphite central electrode to one with an aluminum central electrode. The CPU times are shown for a single execution of each user-code, therefore the time for the CAVRZnrc run represents the time taken to perform the calculation for one of the two electrode materials. The CSnrc time is the total time taken to obtain the results for both electrode materials. The calculations all use $AP=1$ keV, $AE=512$ keV, and a splitting factor of 130. The CPU times are shown for calculations that used 100 times fewer histories than those which give 0.03% statistics on the cavity doses.

	CSnrc	CAVRZnrc
D_{gas}^{Al} (Gy/fluence)	$4.5003\times10^{-12}\pm0.027\%$	$4.5004\times10^{-12}\pm0.027\%$
D_{gas}^{gr} (Gy/fluence)	$4.4676\times10^{-12}\pm0.027\%$	$4.4677\times10^{-12}\pm0.027\%$
Relative CPU time (s)	1058	964
D_{gr}/D_{Al}	$0.99272\pm0.00011\%$	$0.99273\pm0.00037\%$

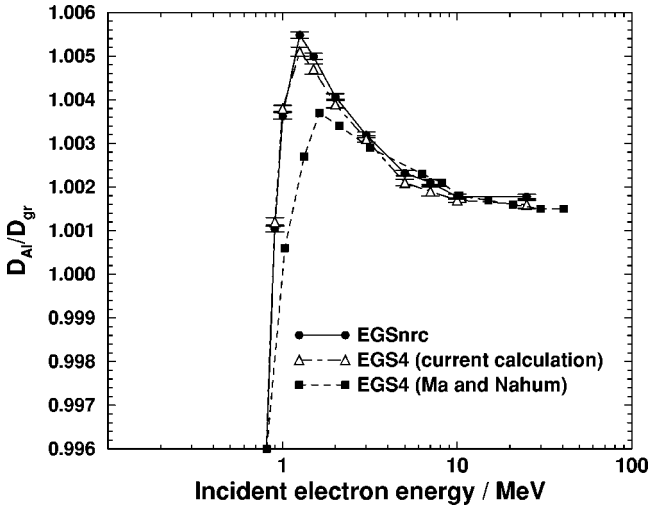

FIG. 5. D_{Al}/D_{gr} for the NE2561 chamber as a function of incident electron energy. The present calculations are performed using monoenergetic electron beams with $AE=521$ keV, $AP=1$ keV, and a splitting factor of 130. The points from Ma and Nahum are digitized from Fig. 5 of their paper (Ref. 7).

$AE=521$ keV and a photon cutoff energy of $AP=1$ keV. The EGS4 calculations are also repeated in the present study, using the same calculation parameters and with ESTEPE $=0.04$ in order to match the value used by Ma and Nahum in their study.

Figure 5 shows the ratio of doses to the cavity D_{Al}/D_{gr} for the NE2561 chamber as a function of incident electron energy. As expected, the presence of the aluminum electrode increases the ionization in the chamber, except for at very low energies, where the electrons cannot penetrate the aluminum electrode. The figure shows close agreement between the CSnrc calculations and the current EGS4 calculations. The EGSnrc calculation for the two electrode materials provided a gain in efficiency of, on average, 15.1 over the same calculation using CAVRZnrc. This is comparable to an average gain of 17.0 when using the EGS4 version of correlated sampling instead of CAVRZ. The gain varied from 12.8 at 0.8 MeV to 16.9 at 25 MeV. The correlation coefficient varied from 0.8724 to 0.9016 over the same energy range. Changes in the EGS4 code since the time of their work may account for some of the difference seen between their results and the current EGS4 calculations. These changes in the code altered the sampling routines for the Møller cross sections and were shown to have noticeable impact on the results for certain applications using high-energy electron beams.[27]

Using the current EGS4 calculations, it is now possible to investigate the assertion of Ma and Nahum, that systematic errors in the absolute dose calculations would cancel in the correlated dose ratio calculation.[5] It has been shown that the absolute doses computed using EGS4 are incorrect, and differ from EGSnrc calculations, by as much as 1%.[14,16] Current calculations show that, in limited situations, the use of correlated sampling improves upon the accuracy of the dose ratio, though the absolute doses are incorrect. Using the NE2561 calculations described above, the absolute doses computed using EGS4 differed from those of EGSnrc by up to 0.8%, whereas the dose ratios D_{Al}/D_{gr} all agree to within 0.02%. However, not all geometries show this cancellation of errors in the dose ratio calculation. The central electrode geometry is one in which the two geometries are highly correlated and the region that varies between geometries, the central electrode, does not contribute greatly to the dose to the cavity. If instead, the chamber wall varies from graphite to aluminum, comparison of current calculations using EGS4 and EGSnrc show that the absolute doses differ by up to 1.7%. In this case, the use of correlated sampling does not improve upon the accuracy of the dose ratio, as the EGS4 value differed from the EGSnrc value by 1.6%. It is therefore not possible, in general, to use correlated sampling in order to compensate for inaccuracies in the dose calculations in older Monte Carlo codes.

B. Ion chamber calculations

1. Central electrode correction in photon beams

Many chambers use an aluminum or a graphite central electrode and therefore the measured ionization must be corrected to account for the change in ionization in the chamber due to the presence of the electrode. The central electrode correction factor P_{cel} is defined as the ratio of ionization in the chamber containing no electrode to that in the chamber containing the electrode. In calculations of this effect, the only part of the simulation geometry that changes is the material of the central electrode. The correlated sampling code is used by specifying the electrode as the correlated sampling region and by executing the code with three options: no electrode, an aluminum central electrode, and a graphite central electrode. The code will then output the ratio of the doses to the cavity for each of two electrode cases against the no electrode geometry, giving values of P_{cel}.

In a previously published work, Ma and Nahum[7] used EGS4 to calculate P_{cel} for a NE2571 ion chamber in-phantom. For the purpose of comparison with their work, the same geometry is employed in the present CSnrc calculations. The chamber is modeled to have an air cavity 6.30 mm in diameter and 24.1 mm in length. The thickness of the graphite walls is 510 mg/cm^2. Ma and Nahum used a simplified NE2571 geometry, so the 1 mm diameter aluminum electrode extends the entire length of the air cavity. In accordance with their calculations, a cylindrical water phantom is used, with a radius of 5 cm for all beams except for the 24 MV beam, for which the radius of the phantom was 7 cm. The calculations use the ^{60}Co spectrum used above[26] and the published spectra from Mohan *et al.*[28] for all other photon beams. All current calculations are performed with $AE=521$ keV and with a photon splitting factor of 100.

Columns 2 and 3 of Table IV show the results of the central electrode calculations for the simplified NE2571 geometry with an aluminum electrode. The present CSnrc results are shown alongside the results of Ma and Nahum[7] which tend to be 0.1% to 0.4% greater than the present calculations. Compared with CAVRZnrc for these calculations,

TABLE IV. The central electrode correction factor P_{cel} for an NE2571 chamber having a 1 mm diameter aluminum electrode. The chamber is placed in a water phantom and is irradiated by high-energy photons. The simplified geometry uses a cylindrical phantom and a variation on the electrode length as described in the text, and is shown here for the purposes of comparison with previously published results from Ma and Nahum.[7] For the 24 MV beam, the chamber is at a depth of 7 cm in the phantom and is at 5 cm depth for all other energies, in this geometry. The real NE2571 geometry includes a chamber stem and uses a $30\times30\times30$ cm^3 cubic water phantom. For the real geometry, the chamber is at a depth of 10 cm in the water phantom for all beams. All current calculations use $AE=521$ keV and a photon splitting factor of 100. The uncertainty on the final digit is shown in parentheses beside each value.

	P_{cel} simplified NE2571		P_{cel}, real NE2571
Beam descriptor	Ma and Nahum[a]	CSnrc	CSnrc
^{60}Co	0.9926(15)	0.9923(1)	0.9924(3)
4 MV	0.9935(7)	0.9920(1)	0.9927(3)
6 MV	0.9930(1)	0.9920(1)	0.9942(6)
10 MV	0.9945(9)	0.9915(1)	0.9945(5)
15 MV	0.9955(16)	0.9918(1)	0.9946(4)
24 MV	0.9957(9)	0.9919(1)	0.9948(3)

[a]Reference 7.

CSnrc results in an efficiency gain that varies from 21 for a ^{60}Co beam to 33 for a 24 MV beam. The fractional increase in computation time for the additional geometry α was between 0.004 and 0.02 for these calculations.

Given the present availability of computing power and the added correlated sampling variance reduction technique, it is feasible to repeat these in-phantom calculations of the electrode correction for a more realistic geometry. The geometry in this case is the actual NE2571 geometry, wherein the electrode has a length of 20.6 mm, and the chamber is placed in a $30\times30\times30$ cm^3 cubic water phantom, as is used in standard dosimetry practice. The chamber is placed at 10 cm depth within the phantom and a 10×10 cm^2 photon field is incident on the phantom. The chamber is modeled to include the stem, as described elsewhere.[29] Using the same photon beams as above, the values of P_{cel} for the NE2571 chamber in-phantom are shown in the last column of Table IV. The values change by up to 0.3% from the simplified geometry, but these changes nearly offset the differences with the original results of Ma and Nahum.

These calculations of P_{cel} for the detailed NE2571 geometry in a water phantom may be compared to the values of P_{cel} currently used in dosimetry protocols. Figure 6 shows the value of P_{cel} as a function of $\%dd_x(10)$, for both graphite and aluminum electrodes, in comparison to the values currently used in the TG-51 protocol.[19] The TG-51 values are based upon the calculations of Ma and Nahum described above.[7] The current calculations significantly reduce the uncertainty on the value of P_{cel} and agree with the values used by TG-51 to within 0.04%, with the exception of the 85% point which shows a 0.1% difference. The IAEA protocol[20] uses values of P_{cel} for photon beams based upon the same calculations from Ma and Nahum and their values do not differ significantly from the TG-51 values.

2. Central electrode correction for high energy electron beams

The value of P_{cel} for a chamber with a 1 mm diameter aluminum electrode in electron beams differs somewhat depending on the dosimetry protocol used. The IAEA's TRS-398 code of practice[20] uses a value of $P_{cel}=0.998$ for all electron beam energies, with an estimated uncertainty of 0.1%. This value is based upon the calculations of Ma and Nahum[7] and upon the much less precise measurements of Palm and Mattsson.[25] Based upon the calculations of Ma and Nahum,[7] the AAPM's TG-51 dosimetry protocol[19] uses a value of $P_{cel}=1.000$ for beam energies less than 13 MeV and a value of $P_{cel}=0.998$ for beam energies greater than 13 MeV.[30] Rather than a discontinuity, TG-51 uses a smoothed interpolation between the two values of P_{cel} in order to use it in the calculation of the beam quality conversion factor $k'_{R_{50}}$.

Using CSnrc, it is now possible to calculate the central electrode correction factor P_{cel} for an NE2571 chamber in electron beams with much lower uncertainty than previously achieved. It is also feasible to perform the calculations for several realistic electron beam spectra, whereas the values

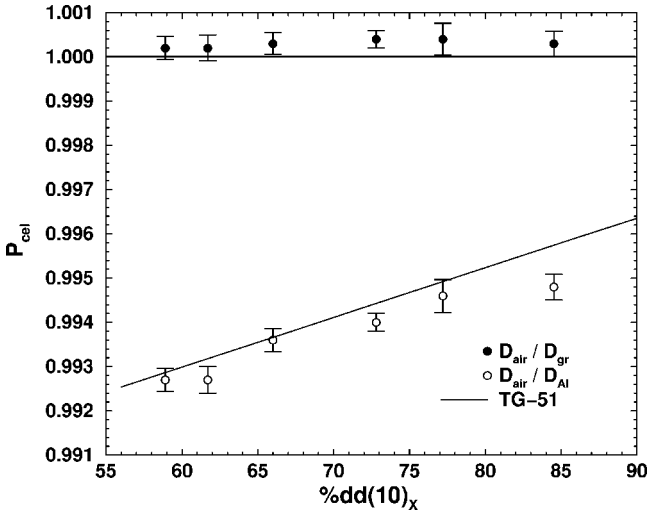

FIG. 6. The central electrode correction factor P_{cel} for a realistic NE2571 ionization chamber in photon beams. The CSnrc values are computed with the chamber in a $30\times30\times30$ cm^3 water phantom. The calculations are for a 1 mm diameter central electrode. The remaining geometry details are described in the text. The Monte Carlo values are shown along with the curve used in the TG-51 dosimetry protocol (Ref. 19). All CSnrc calculations use $AE=521$ keV and $AP=1$ keV.

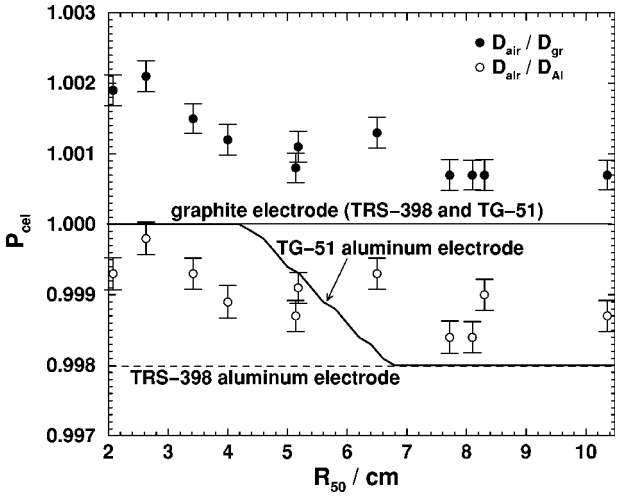

FIG. 7. The central electrode correction factor P_{cel} for a realistic NE2571 ionization chamber in electron beams. The CSnrc values are computed with the chamber placed at a depth of d_{ref} in a $30\times30\times30$ cm^3 water phantom. The calculations are for a 1 mm diameter central electrode. The Monte Carlo calculations are shown along with the values of P_{cel} used in the AAPM's TG-51 protocol (Ref. 19) and in the IAEA's TRS-398 code of practice (Ref. 20). All calculations use $AE=521$ keV and $AP=1$ keV.

used in protocols are based upon the three beam energies and several discrete depths considered in the EGS4 calculations. The present calculations use the real NE2571 geometry described above in a rectangular $30\times30\times30$ cm^3 water phantom. The incident spectra are taken from Ding and Rogers[31] for beams with nominal energy ranging from 5 to 25 MeV. For all beams, the chamber is placed at a depth of d_{ref} in the phantom.

Figure 7 shows the CSnrc calculated values of P_{cel} as a function of the beam quality specifier R_{50}. The values of R_{50} for the realistic beams considered here are taken from Ding and Rogers.[31] The CSnrc values are computed to 0.02% statistical uncertainty. These values are shown along with the current values of P_{cel}, as used in TG-51 and TRS-398. Both protocols use a correction factor of 1.000 for a graphite electrode. However, the current calculations show that for lower beam energies, the correction is as much as 0.2% for a graphite electrode. The calculations using the aluminum electrode show approximately a 0.1% difference from the value of $P_{cel}=0.998$ used by the TRS-398 code of practice for all beam energies. Similarly, there is on the order of a 0.1% difference between the current calculations and the values used in the AAPM's TG-51 protocol.

IV. CONCLUSIONS

A correlated sampling dose scoring user-code has been implemented based on the EGSnrc Monte Carlo system. This method reduces the total time needed for simulations of multiple geometries and reduces the statistical uncertainties on ratios of calculated quantities by exploiting correlations between the geometries. The development of an EGSnrc correlated sampling user-code CSnrc from an existing user-code CAVRZnrc has been described. CSnrc includes a rectangular phantom geometry and the option to vary the photon cross sections by a user-specified amount: two options not currently available in CAVRZnrc. CSnrc is based upon an earlier correlated sampling code,[5] developed by Ma and Nahum for use with the EGS4 Monte Carlo code. The correlated sampling algorithm has been changed from the EGS4 version such that there is no unnecessary repetition of particle transport and the code is now compatible with the existing EGSnrc source code without requiring changes to the EGSnrc system.

The CSnrc code has been benchmarked against pairs of simulations using CAVRZnrc. For ion chamber calculations, the doses to the cavity computed by the two codes have been shown to agree within statistical uncertainties. For the range of geometries considered in the present paper, CSnrc was shown to improve upon the efficiency of dose ratio calculations by up to a factor of 64 for a single additional geometry. For typical thimble ionization chamber calculations, the gain in efficiency was between 1.5 and 64 when using correlated sampling.

The CSnrc code has been used to compute the central electrode effect in a thimble chamber in a variety of photon beams and in high-energy electron beams. With the present code, it is possible to achieve very low uncertainties on the electrode correction factors, both in phantom and in air. For photon beams, there is no significant difference between the present values of P_{cel} and the values used in current dosimetry protocols. For electron beams the difference between the current values of P_{cel} and those used in the dosimetry protocols is on the order of 0.1% for an aluminum central electrode and is up to 0.2% for a graphite electrode. CSnrc calculations using an aluminum central electrode show that P_{cel} has a value slightly larger than the constant value of 0.998 used by the IAEA code of practice for all beam energies.[20] Also, the values of P_{cel} as a function of energy do not show as much variation with energy as indicated by the TG-51 protocol[19] which uses values of P_{cel} of 1.000 to 0.998.

ACKNOWLEDGMENTS

The authors wish to thank their colleagues at the National Research Council of Canada: Ernesto Mainegra-Hing for his assistance in implementing the photon cross-section variability into the CSnrc code, and Malcolm McEwen for valuable suggestions regarding this manuscript. L.B. would like to acknowledge support from the Natural Sciences and Engineering Research Council of Canada.

[a]Electronic mail: lbuckley@irs.phy.nrc.ca

[1]B. Nilsson, A. Montelius, P. Andreo, and B. Sorcini, "Perturbation correction factors in ionization chamber dosimetry," in *Dosimetry in Radiotherapy* (IAEA, Vienna, 1988), Vol. 1, pp. 175–185.
[2]P. Andreo, L. Linborg, and J. Medin, "On the calibration of plane-parallel ionization chambers using ^{60}Co beams," Med. Phys. **18**, 326–327 (1991).
[3]A. F. Bielajew and D. W. O. Rogers, "Variance-reduction techniques," in *Monte Carlo Transport of Electrons and Photons*, edited by T. M. Jenkins, W. R. Nelson, A. Rindi, A. E. Nahum, and D. W. O. Rogers (Plenum Press, New York, 1988), pp. 407–419.
[4]I. Kawrakow and M. Fippel, "Investigation of variance reduction techniques for Monte Carlo photon dose calculation using XVMC," Phys. Med. Biol. **45**, 2163–2184 (2000).
[5]C.-M. Ma and A. E. Nahum, "Calculation of absorbed dose ratios using

correlated Monte Carlo sampling," Med. Phys. **20**, 1189–1199 (1993).
[6]C.-M. Ma and A. E. Nahum, "A correlated sampling method for Monte Carlo radiation transport and its implementation is the EGS4 code system," Technical Report PIRS-421, National Research Council of Canada, Ottawa, Canada, 1994.
[7]C. M. Ma and A. E. Nahum, "Effect of size and composition of the central electrode on the response of cylindrical ionization chambers in high-energy photon and electron beams," Phys. Med. Biol. **38**, 267–290 (1993).
[8]C.-M. Ma, D. W. O. Rogers, K. R. Shortt, C. K. Ross, A. E. Nahum, and A. F. Bielajew, "Wall correction and absorbed dose conversion factors for Fricke dosimetry: Monte Carlo calculations and measurements," Med. Phys. **20**, 283–292 (1993).
[9]C.-M. Ma and A. E. Nahum, "Monte Carlo calculated stem effect corrections for NE2561 and NE2571 chambers in medium-energy x-ray beams," Phys. Med. Biol. **40**, 63–72 (1995).
[10] M. A. Holmes, T. R. Mackie, W. Sohn, P. J. Reckwerdt, T. J. Kinsella, A. F. Bielajew, and D. W. O. Rogers, "The application of correlated sampling to the computation of electron beam dose distributions in heterogeneous phantoms using the Monte Carlo method," Phys. Med. Biol. **38**, 675–688 (1993).
[11]A. F. Bielajew, "Correction factors for thick-walled ionization chambers in point-source photon beams," Phys. Med. Biol. **35**, 501–516 (1990).
[12]H. Hedtjärn, G. Carlsson, and J. Williamson, "Accelerated Monte Carlo based dose calculations for brachytherapy planning using correlated sampling," Phys. Med. Biol. **47**, 351–376 (2002).
[13]I. Lux and L. Koblinger, *Monte Carlo Particle Transport Methods: Neutron and Photon Calculations* (CRC Press, New York, 1991).
[14]I. Kawrakow, "Accurate condensed history Monte Carlo simulation of electron transport. I. EGSnrc, the New EGS4 version," Med. Phys. **27**, 485–498 (2000).
[15]I. Kawrakow and D. W. O. Rogers, "The EGSnrc code system: Monte Carlo simulation of electron and photon transport," Technical Report PIRS-701, National Research Council of Canada, Ottawa, Canada, 2000 (see http://www.irs.inms.nrc.ca/inms/irs/EGSnrc/EGSnrc.html).
[16]I. Kawrakow, "Accurate condensed history Monte Carlo simulation of electron transport. II. Application to ion chamber response simulations," Med. Phys. **27**, 499–513 (2000).
[17]D. W. O. Rogers, I. Kawrakow, J. P. Seuntjens, and B. R. B. Walters, "NRC user codes for EGSnrc," Technical Report PIRS-702, National Research Council of Canada, Ottawa, Canada, 2000.
[18]W. R. Nelson, H. Hirayama, and D. W. O. Rogers, "The EGS4 code system," Report SLAC-265, Stanford Linear Accelerator Center, Stanford, California, 1985.
[19]P. R. Almond, P. J. Biggs, B. M. Coursey, W. F. Hanson, M. S. Huq, R. Nath, and D. W. O. Rogers, "AAPM's TG-51 protocol for clinical reference dosimetry of high-energy photon and electron beams," Med. Phys. **26**, 1847–1870 (1999).
[20]IAEA, "Absorbed dose determination in external beam radiotherapy: An international code of practice for dosimetry based on standards of absorbed dose to water," Vol. 398 of *Technical Report Series*, IAEA, Vienna, 2001.
[21]I. Kawrakow, E. Mainegra-Hing, and D. W. O. Rogers, "EGSnrcMP: The multi-platform environment for EGSnrc," Technical Report PIRS-877, National Research Council of Canada, Ottawa, Canada, 2003.
[22]E. Mainegra-Hing, I. Kawrakow, and D. W. O. Rogers, "Calculations for plane-parallel ion chambers in ^{60}Co beams using the EGSnrc Monte Carlo code," Med. Phys. **30**, 179–189 (2003).
[23]B. R. B. Walters, I. Kawrakow, and D. W. O. Rogers, "History by history statistical estimators in the BEAM code system," Med. Phys. **29**, 2745–2752 (2002).
[24]L. A. Buckley, I. Kawrakow, and D. W. O. Rogers, "An EGSnrc investigation of cavity theory for ion chambers measuring air kerma," Med. Phys. **30**, 1211–1218 (2003).
[25]A. Palm and O. Mattsson, "Experimental study on the influence of the central electrode in farmer-type ionization chambers," Phys. Med. Biol. **44**, 1299–1308 (1999).
[26]G. Mora, A. Maio, and D. W. O. Rogers, "Monte Carlo simulation of a typical ^{60}Co therapy source," Med. Phys. **26**, 2494–2502 (1999).
[27]A. F. Bielajew and D. W. O. Rogers, "Effects of a Møller cross section error in the EGS4 code," Med. Phys. **23**, 1153 (1996).
[28]R. Mohan, C. Chui, and L. Lidofsky, "Energy and angular distributions of photons from medical linear accelerators," Med. Phys. **12**, 592–597 (1985).
[29]E. G. A. Aird and F. T. Farmer, "The design of a thimble chamber for the Farmer dosimeter," Phys. Med. Biol. **17**, 169–174 (1972).
[30]D. W. O. Rogers, "Fundamentals of dosimetry based on absorbed-dose standards," in *Teletherapy Physics, Present and Future*, edited by J. R. Paltaand T. R. Mackie, AAPM, Washington DC, 1996, pp. 319–356.
[31]G. X. Ding and D. W. O. Rogers, "Energy spectra, angular spread, and dose distributions of electron beams from various accelerators used in radiotherapy, " Report PIRS-0439, National Research Council of Canada, Ottawa, Canada, 1995 (see http://www.irs.inms.nrc.ca/inms/irs/papers/PIRS439/pirs439.html).